Table 1
Measured 662 keV energy resolutions (FWHM) of the pixels in each readout system

System	Best (%)	Typical (%)	Worst (%)
CP80068	8.9	9.5	10.0
16 ch readout	8.0	8.7	9.5
Four ch readout	8.6	8.8	9.9

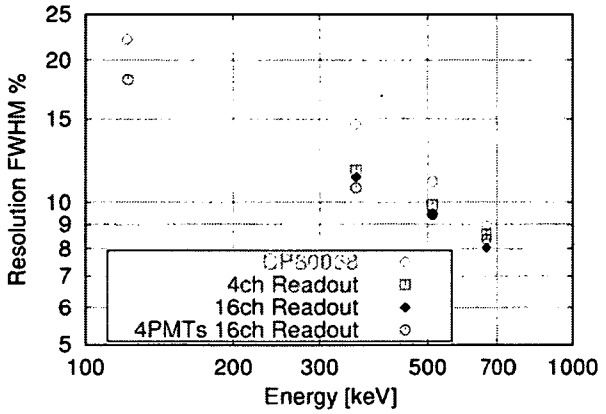

Fig. 5. Measured energy resolution of the best pixels of all the readout systems. Results of "4PMTs 16 ch Readout" explained in Fig. 6 are also indicated.

For further reduction of the readout channels, we connected the intervals of the both edges of the horizontal chains with 100 Ω resistors, thus four channels readout with resistive chain is also tested.

4. Measurements and results

We are interested in the energy of sub-MeV region [5], accordingly, the CsI(Tl) array was irradiated by 1 MBq ^{137}Cs source (662 keV) at a distance of 30 cm. For the energy calibration, ^{22}Na (511 keV), ^{133}Ba (356 keV) and ^{57}Co (122 keV) were also used. An important point to mention here is the dynamic ranges of the readout circuits. As the input dynamic range of CP80068 is as small as −15 pC, H8500 should be operated with the gain of 10^4 (HV~600 V) to observe 662 keV gamma rays. In the case of resistive charge division circuits, dynamic ranges of the shaper and the ADC also limit the operation gain of H8500 to 10^5 (HV~800 V).

4.1. Spatial resolution

The obtained flood irradiation images of ^{137}Cs are shown in Fig. 4. The methods of the calculation of the position reconstruction are indicated as well. Image spots represent pixels of the CsI(Tl) array, which indicates that the intrinsic spatial resolution of H8500 is better than the anode pixel size.

The accidental hit events of multi-pixels were rejected in the results of CP80068 system (selection efficiency was

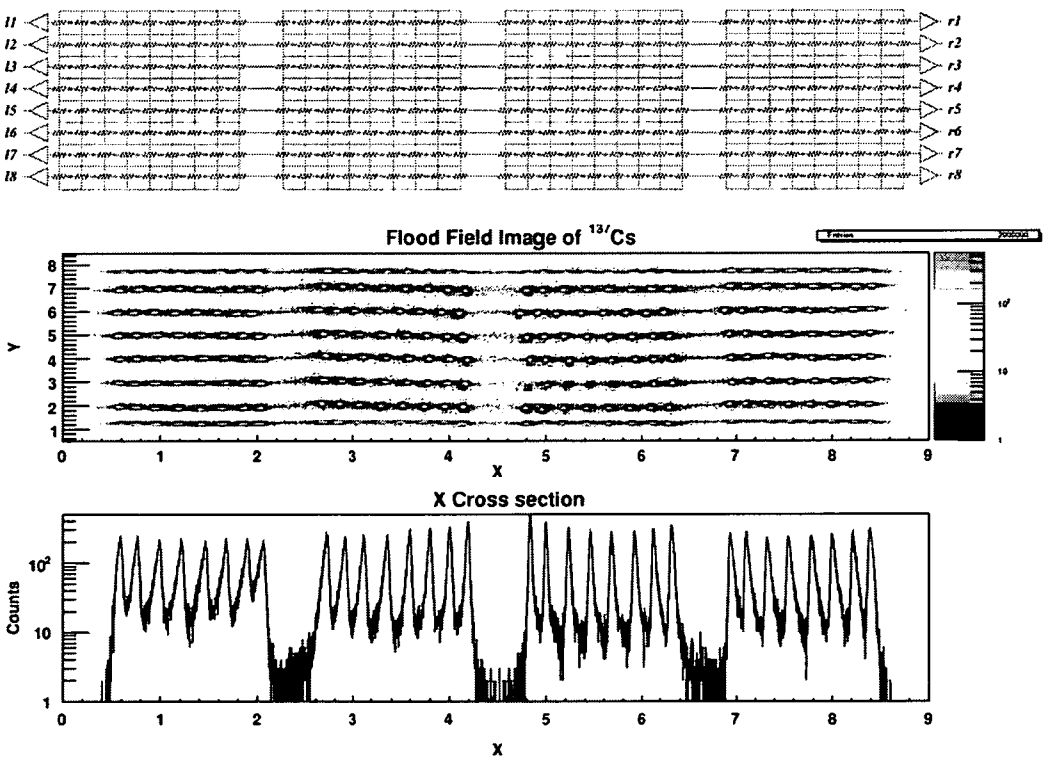

Fig. 6. Cascade connection of four H8500s with resistive charge divider network.

79%) and the accidental hit events of more than two horizontal rows were also rejected in the results of the 16 channels readout system (selection efficiency was 85%). On the other hand, in the four channels readout system, there is no way to reject such events; therefore, the peak to valley ratios of the x/y cross-section of the flood irradiation image are the worst.

4.2. Energy resolution

The obtained energy spectra of the best pixel of each readout system are also shown in Fig. 4. The variations of the energy resolution of 662 keV of every readout system are summarized in Table 1.

The variation of the resolution is mainly due to the variation of the anode gain. Near the boundary of the detection area, optical leakage (photon collection inefficiency) also affects not only the energy resolution but also the spatial resolution. Fig. 5 shows the energy resolutions of measured energy of all the readout systems. The reason why the energy resolution of the result of CP80068 system is the worst is its low HV operation.

5. Discussion and conclusion

It is admitted that individual anode readout is the best way for multi-anode PMTs, however, that needs development of exclusive ASICs with consideration for the light outputs of scintillator, gain of the PMT, and the dynamic range. Moreover, in our case, the spatial resolution is not determined by the anode pixel size but by the crystal pixel size.

Therefore, the advantage of energy resolution of the resistive charge divider network and discrete modules of readout circuit is encouraging to make larger area detector. We made cascade resistive connection of four H8500s as shown in Fig. 6, for example. The energy resolution is also shown in Fig. 5. This connection is another example of four channels/PMT readout and crystal pixel identification is better than that of previous four channels readout system.

In conclusion, large area detector of pixel scintillator and H8500 array with resistive charge division systems have a good performance both energy and spatial resolutions and have many possibilities in medical and gamma ray astronomy applications.

Acknowledgement

We would like to thank Takahashi Lab. at Institute of Space and Astronautical Science, Japan Aerospace Exploration Agency, Makishima Lab. at Department of Physics, School of Science, University of Tokyo and Dr. Gunji for the development of CP80068.

References

[1] Hamamatsu technical data sheet H8500-H8500B, H9500, February 2005, printed in Japan, (http://www.hamamatsu.com).
[2] R. Pani, et al., Nucl. Instr. and Meth. A 527 (2004) 54;
R. Pani, et al., Nucl. Instr. and Meth. A 513 (2003) 36.
[3] M. Giménez, et al., Nucl. Instr. and Meth A 525 (2004) 298.
[4] D. Herbert, et al., Nucl. Instr. and Meth. A 518 (2004) 399.
[5] A. Takada, et al., Nucl. Instr. and Meth. A 546 (2005) 258.
[6] G. Kanbach, et al., Nucl. Instr. and Meth. A 541 (2005) 310.
[7] A. Studen, et al., Nucl. Instr. and Meth. A 531 (2004) 258.
[8] T. Tanimori, et al., New Astron. Rev. 48 (2004) 263.
[9] ROOT, An object-oriented analysis framework, (http://root.cern.ch).

資料 16

資料(17)

資料 17

Available online at www.sciencedirect.com
ScienceDirect
ELSEVIER
Nuclear Instruments and Methods in Physics Research A 573 (2007) 115–118
NUCLEAR INSTRUMENTS & METHODS IN PHYSICS RESEARCH Section A
www.elsevier.com/locate/nima

Development of large area gamma-ray camera with GSO(Ce) scintillator arrays and PSPMTs

H. Nishimura[a,*], K. Hattori[a], S. Kabuki[a], H. Kubo[a], K. Miuchi[a], T. Nagayoshi[b], Y. Okada[a], R. Orito[c], H. Sekiya[a], A. Takada[a], A. Takeda[d], T. Tanimori[a], K. Ueno[a]

[a]*Department of Physics, Graduate School of Science, Kyoto University, Kitashirakawa-oiwake, Sakyo, Kyoto 606-8502, Japan*
[b]*Advanced Research Institute for Science and Engineering, Waseda University, 17 Kikui-cho, Shinjyuku, Tokyo 162-0044, Japan*
[c]*Department of Physics, Graduate School of Science and Technology, Kobe University, 1-1 Rokkoudai, Nada, Kobe 657-8501, Japan*
[d]*Kamioka Observatory, ICRR, University of Tokyo, 456 Higasi-mozumi, Hida-shi, Gifu 506-1205, Japan*

Available online 29 November 2006

Abstract

We have developed a position-sensitive scintillation camera with a large area as an absorber of an advanced Compton gamma-ray camera. At first we tested GSO(Ce) crystals. We compared light output from the GSO(Ce) crystals under various conditions: the method of surface polishing, the concentration of Ce, and co-doping Zr. As a result, we chose the GSO(Ce) crystals doped only 0.5 mol% Ce, surface of which was polished by chemical etching for the scintillator of our camera. We also made a $16 \times 16\,cm^2$ scintillation camera which consisted of nine position-sensitive PMTs (PSPMTs Hamamatsu flat-panel H8500), the each of which had 8×8 anodes with a pitch of 6 mm and coupled to 8×8 arrays of pixelated $6 \times 6 \times 13\,mm^3$ GSO(Ce) scintillators. For the readout system of 576 anodes of the PMTs, we used chained resistors to reduce the number of readout channels down to 48 for saving power consumption. The camera has the position resolution of less than 6 mm and a typical energy resolution of 10.5% (FWHM) at 662 keV at each pixel in a large area of $16 \times 16\,cm^2$.

Furthermore, we constructed a 16×16 array of $3 \times 3 \times 13\,mm^3$ pixelated GSO(Ce) scintillators, and glued it to a PMT H8500. This camera had the position resolution of less than 3 mm in area of $5 \times 5\,cm^2$, except for some of edge pixels; the energy resolution was typically 13% (FWHM) at 662 keV.

PACS: 85.60.Ha; 87.58.Pm; 95.55.Ka

Keywords: GSO(Ce); Gamma-ray camera; PSPMTs

1. Introduction

We have been developing an advanced Compton camera for gamma-ray astronomy in the range of 100 keV to 20 MeV [1]. It needs a scintillation camera as a detector for Compton-scattered gamma rays, which has good energy and position resolution and a large area because the resolution and the efficiency for the scattered gamma rays contribute to the angular resolution and the efficiency of the advanced Compton camera. In addition, radiation hardness and a high counting-rate performance of the scintillation camera are required. For these requirements, we chose a GSO(Ce) (Gd_2SiO_5 : Ce) crystal as a scintillator, and the PSPMT H8500 (Flat Panel PMT produced by Hamamatsu [2]) as a position-sensitive photon device.

GSO(Ce) has advantages in astronomical use, such as having a higher-Z, faster decay time than NaI(Tl), a higher light output than BGO, greater radiation hardness and less radioactivation than most of the known scintillators. Furthermore, GSO(Ce) can be easily cut and polished, since it is nonhydroscopic.

The PSPMT H8500 was recently developed as a promising device for nuclear physics and medicine, for example, PET and SPECT [3–6]. It has 8×8 anodes with a 6 mm pitch and 12-stage metal channel dynodes. The

*Corresponding author. Tel.: +81 75 753 3869; fax: +81 75 753 3799.
E-mail address: nisimura@cr.scphys.kyoto-u.ac.jp (H. Nishimura).

0168-9002/$ - see front matter © 2006 Elsevier B.V. All rights reserved.
doi:10.1016/j.nima.2006.11.029

advantage of this PMT is that it has a much smaller dead space and a larger effective area than that of the previous multi-anode PMTs. The effective area of this PMT is $49 \times 49\,mm^2$, which is 89% of the package size.

In this paper we report on the result of measurements of pixelated GSO(Ce) scintillators and the performances (energy resolution and position resolution) of our developed scintillation camera.

2. Measurements of pixelated GSO(Ce) scintillators

There are some conditions that characterize the performance of a pixelated GSO(Ce) scintillator. One is the pixel size. The width of 6 mm and the thickness of 13 mm were chosen for our scintillation camera in order to fit the pitch of the anodes of PSPMTs, and the radiation length. One of the other important issues is the method of surface polishing. There are two established methods of polishing: one is chemical etching, and the other is mechanical polishing. It was reported that there was little difference between the performances of pixelated scintillators polished with these methods [7]. However, mechanical polishing is more expensive than chemical etching. Another important issue is the concentration of Ce as a scintillation activity impurity, and additional dopants. The light-decay time becomes faster as the concentration of Ce increases, although increasing the concentration of Ce decreases the optical transmittance of the crystal. It was also reported that doping 200 ppm of Zr to GSO(Ce) improved the optical transmittance of the crystal [8].

We measured the light outputs from several crystals under different conditions of polishing or doping impurity in order to examine how effective these conditions were. There were eight types of pixelated scintillators, which were different at the point of the concentration of Ce, the existence of Zr, and the ingot. We enveloped each pixel scintillator by a reflector (Goatex) and coupled the crystal face with an area of $6 \times 6\,mm^2$ or $4 \times 6\,mm^2$ to a single anode PMT (R6231 Hamamatsu) with the optical grease (OKEN 6262). We then irradiated it with 662 keV gamma rays from a ^{137}Cs source through a $\varnothing 3$ mm collimator. Fig. 1 shows the relative light outputs and energy resolution at 662 keV. The systematic errors were due to the reproducible errors of the condition of crystal with the reflector or the condition of gluing. It shows that the method of polishing and the optical transmittance caused by the concentration of Ce are not more effective for the performance of our pixel size of $6 \times 6 \times 13\,mm^3$ than the difference of the ingot. However, there is a significant difference between only 1 mol% Ce doped crystals with a size of $4 \times 6 \times 20\,mm^3$ and the others. This shows a significant decreasing of the optical transmittance caused by Ce and the improvement of transmittance caused by doping Zr for longer crystal with a thickness of 20 mm.

From the above studies, we chose crystals that were polished by chemical etching and doped only Ce-0.5 mol% for our camera. We made an 8×8 array of pixelated GSO(Ce) scintillators. Each pixel was optically separated by Vikuiti 3M ESR, which is a multilayer polymer mirror with a thickness of 65 μm and a reflectance of 98%. The construction of this array is described in Ref. [6].

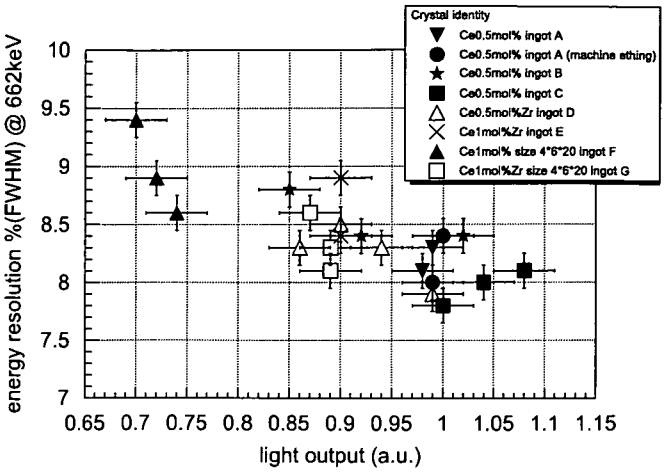

Fig. 1. Light output and energy resolution of pixelated GSO(Ce) scintillators with or without a Zr dopant. The systematic errors are also shown.

3. Performance of a $5 \times 5\,cm^2$ scintillation camera and a $16 \times 16\,cm^2$ scintillation camera

We made a $5 \times 5\,cm^2$ scintillation camera by coupling an 8×8 GSO(Ce) array to a PMT H8500 with grease. In order to save power consumption, the readout circuit of the camera consisted of eight resistive chains, 16 ch amplifiers, and ADCs, as described in Ref. [9].

The image of each pixel scintillator was clearly resolved by a flood field of irradiation of 662 keV gamma ray, which means that the position resolution was less than a pixel pitch of 6 mm. Furthermore, we also obtained the energy spectrum of each pixel with energy resolution of 10% (FWHM) @ 662 keV.

This $5 \times 5\,cm^2$ camera can be easily extended to a larger camera. We constructed a $16 \times 16\,cm^2$ camera with 3×3 PMTs, as shown in Fig. 2. The pitch of PMTs was 53 mm and the effective area of the camera is 82%. The number of readout channels of the camera was only 48 channels with 24 resistive chains. All 576 pixels were clearly resolved by a flood field of radiation of 662 keV gamma ray, as shown in Fig. 3(a) and (b), which are an event map and an x-projection map at the 12th row ($78\,mm < y < 84\,mm$), respectively. The events located between each pixels seem to be multi-pixel hits events by Compton-scattered gamma ray or accidental events. The energy resolution (FWHM) was 31.0% at 122 keV, 18.2% @356 keV, 13.9% @511 keV, 10.7% @662 keV, 9.6% @835 keV, 8.6% @1173 keV for the typical pixel, 9.8%@662 keV(FWHM) for good pixels and 13%@662 keV(FWHM) for bad pixels. Fig. 4 shows a map of the relative light output at each pixel. It mainly shows differences among anode

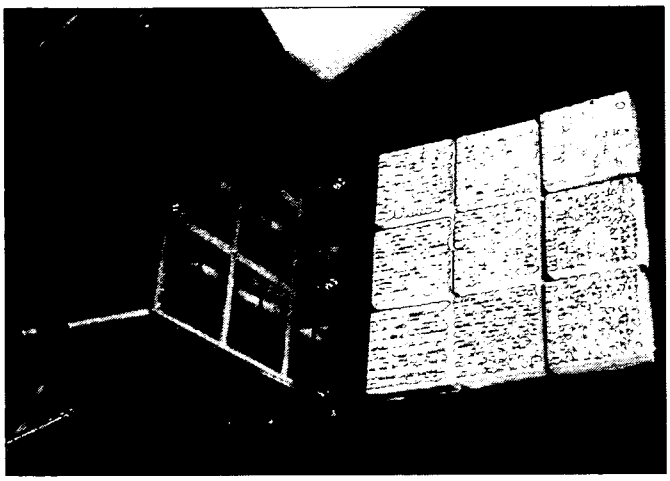

Fig. 2. Photograph of a $16 \times 16\,cm^2$ scintillation camera composed of nine PSPMTs, the each of which coupled to 8×8 arrays of pixelated $6 \times 6 \times 13\,mm^3$ GSO(Ce) crystals.

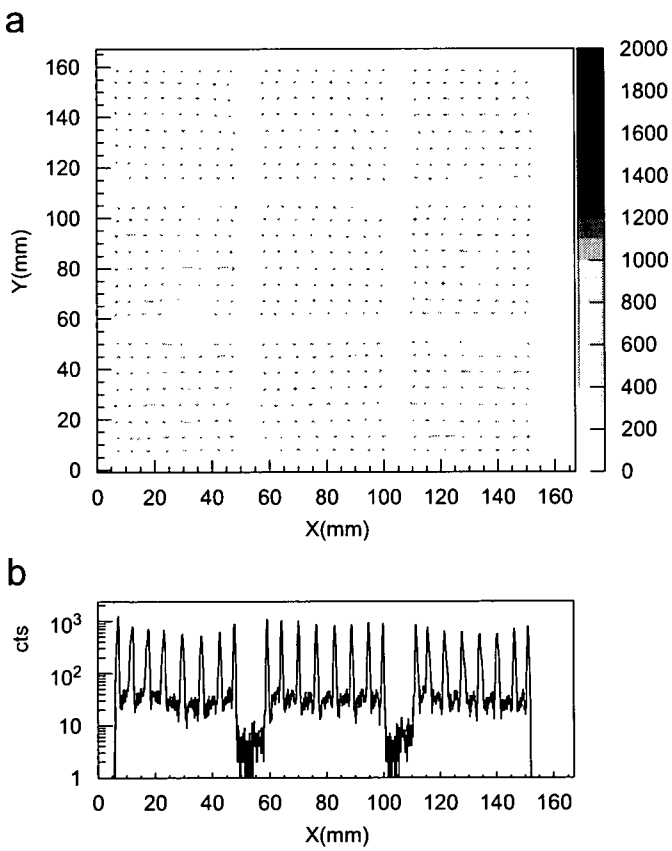

Fig. 3. (a) Event map measured with the $16 \times 16\,cm^2$ scintillation camera in a flood of irradiation of 662 keV gamma rays. (b) The logarithmic x-projection of the event map at the 12th row ($78\,mm < y < 84\,mm$).

gains of the PMTs. However, the light output was too low at some edges of each PMT. This was probably due to a misalignment of the array of crystals to the PMTs. The measurable energy ranges of this camera are 80–1300 keV and 100–900 keV, at good and bad pixels, respectively.

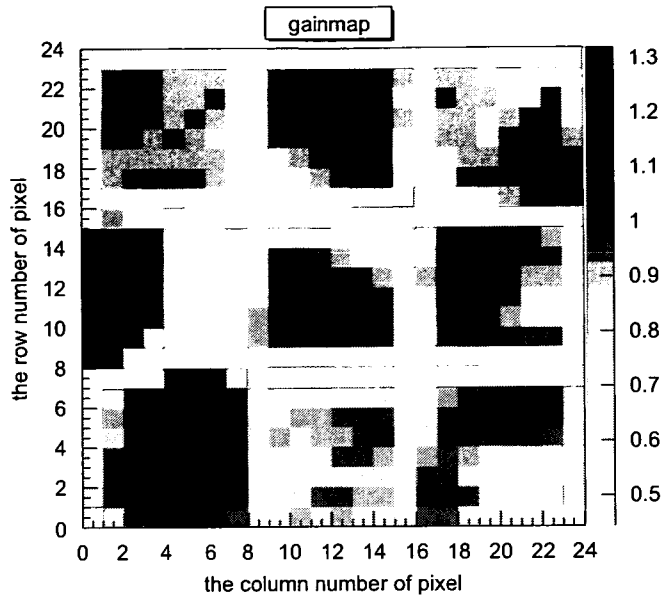

Fig. 4. Distribution of the light outputs for the $16 \times 16\,cm^2$ scintillation camera composed of arrays of $6 \times 6 \times 13\,mm^3$ GSO(Ce) pixelated crystals.

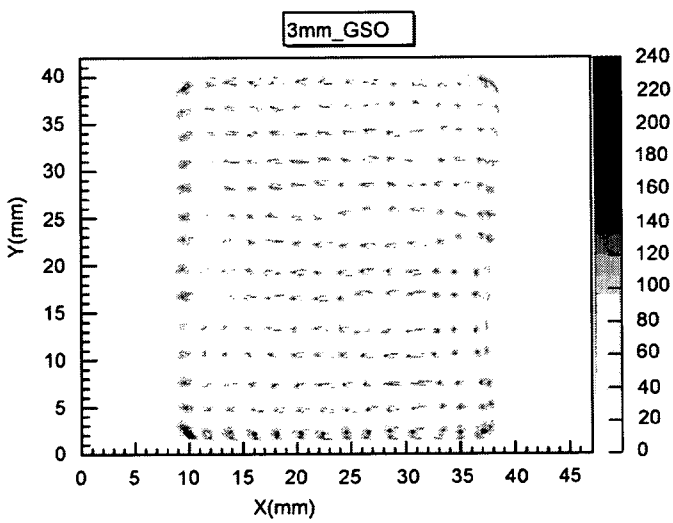

Fig. 5. Event map measured with a scintillation camera composed of a 16×16 array of $3 \times 3 \times 13\,mm^3$ pixelated GSO(Ce) crystals and a H8500.

In order to improve the position resolution, we tried to use smaller pixels with a width of 3 mm compared to that of the anode pitch of H8500. Such developments were already reported by papers [3–5]. We made a 16×16 array of pixelated $3 \times 3 \times 13\,mm^3$ GSO(Ce) scintillators and coupled it to the H8500. In the flood field of irradiation of 662 keV gamma rays, the pixel image was clearly separated, except for some of edge pixels, as shown in Fig. 5. However, the energy resolution became worse to 12% @662 keV than one of scintillation cameras with $6 \times 6 \times 13\,mm^3$ pixels.

4. Summary

We measured the light outputs from GSO(Ce) scintillators under some different conditions, and chose a Zr nondoped chemical etching GSO(Ce) crystal with size of $6 \times 6 \times 13\,mm^3$ for our scintillation camera. We constructed 8×8 arrays of the crystal, and developed a $16 \times 16\,cm^2$ GSO scintillation camera. The performance of this camera is sufficient to use as an Compton-scattered gamma-ray camera of our advanced Compton camera. We have been constructing an advanced Compton camera and testing its performance.

Acknowledgments

This work is supported by a Grant-in-Aid for the 21st Century COE "Center for Diversity and Universality in Physics"; a Grant-in-Aid in Scientific Research of the Japan Ministry of Education, Culture, Science, Sports, Technology; "SENTAN", JST. We thank Dr. Y. Yanagida and Hitachi Chemical, Co. Ltd. for their support.

References

[1] A. Takada, et al., Nucl. Instr. and Meth. A 546 (2005) 258.
[2] Hamamatsu technical data sheet H8500-H8500B, February 2005, printed in Japan, ⟨http://www.hamamatsu.com⟩.
[3] R. Pani, et al., Nucl. Instr. and Meth. A 527 (2004) 54; Nucl. Instr. and Meth. A 513 (2003) 36.
[4] M. Gimenez, et al., Nucl. Instr. and Meth. A 525 (2004) 298.
[5] D. Herbert, et al., Nucl. Instr. and Meth. A 518 (2004) 399.
[6] N. Inadama, et al., IEEE Trans. Nucl. Sci. NS-51 (1) (2004) 58; IEEE Trans. Nucl. Sci. NS-52(1) (2005) 15.
[7] K. Kurashige, et al., IEEE Trans. Nucl. Sci. NS-45 (3) (1998) 522.
[8] Hitachi, chemical Technical Report No.44 13 (2005-1), Printed in Japan, ⟨http://www.hitachi-chem.co.jp/japanese/report/⟩.
[9] H. Sekiya, et al., Nucl. Instr. and Meth. A 563 (2006) 49.

資料(18)

資料 18

Available online at www.sciencedirect.com
ScienceDirect
ELSEVIER
Nuclear Instruments and Methods in Physics Research A 581 (2007) 517–521
NUCLEAR INSTRUMENTS & METHODS IN PHYSICS RESEARCH Section A
www.elsevier.com/locate/nima

Gamma-ray imaging with a large micro-TPC and a scintillation camera

K. Hattori[a,*], S. Kabuki[a], H. Kubo[a], S. Kurosawa[a], K. Miuchi[a], T. Nagayoshi[b], H. Nishimura[a], Y. Okada[a], R. Orito[c], H. Sekiya[a], A. Takada[a], A. Takeda[d], T. Tanimori[a], K. Ueno[a]

[a]*Graduate School of Science, Department of Physics, Kyoto University Kitashirakawa, Sakyo, Kyoto 606-8502, Japan*
[b]*Advanced Research Institute for Science and Engineering, Waseda University, 17 Kikui-cho, Shinjuku 162-0044, Tokyo, Japan*
[c]*Graduate School of Science and Technology, Department of Physics, Kobe University, 1-1 Rokkoudai, Nada, Kobe 657-8501, Japan*
[d]*Kamioka Observatory, ICRR, University of Tokyo, 456 Higashi-mozumi, Hida-shi, Gifu 505-1205, Japan*

Available online 7 August 2007

Abstract

We report on the development of a large Compton camera with the full reconstruction of the Compton process based on a prototype. This camera consists of two kinds of detectors. One is a gaseous time projection chamber (micro-TPC) for measuring the energy and the track of a Compton recoil electron. The micro-TPC is based on a μ-PIC and a GEM, which are micro-pattern gas detectors (MPGDs). The size of the micro-TPC was 10 cm × 10 cm × 8 cm in the case of the prototype, and we enlarged it to 23 cm × 28 cm × 15 cm. The other detector part is a NaI (Tl) Anger camera for measuring the scattered gamma-ray. With these informations, we can completely reconstruct a Compton event, and determine the direction of the incident gamma-ray, event by event. We succeeded in reconstructing events of incident 662 keV gamma-rays. The measured angular resolutions of the "angular resolution measure" (ARM) and the "scatter plane deviation" (SPD) were 9.3° and 158° (FWHM), respectively.

PACS: 29.40.Cs; 29.40.Gx

Keywords: Compton imaging; Time projection chamber; MeV gamma-ray imaging

1. Introduction

In spite of the successful all-sky survey using COMPTEL [1] on board the Compton Gamma Ray Observatory (CGRO) satellite, the number of celestial objects found in the MeV gamma-ray band was smaller by an order of magnitude than that found in the GeV band. Thus, a Compton telescope with improved detection sensitivity is desired. Since the direction of a Compton recoil electron was not measured with COMPTEL, the direction of the incident photon could only be reconstructed as a cone. Accordingly, it was difficult to reject large background, thereby limiting the sensitivity. Measuring the direction of the recoil electron reduces the Compton cone to a small segment of the cone, and realizes the strong background rejection [2,3]. To measure both the three-dimensional track and the energy of the recoil electron, we have developed a gaseous time projection chamber (micro-TPC) based on a "micro-pixel chamber" (μ-PIC), which is a pixel-type two-dimensional imaging detector with a pixel pitch of 400 μm [4]. Both the energy and the direction of the scattered gamma-ray are measured using a NaI(Tl) scintillation camera. Through these measurements, the direction and the energy of the incident gamma-ray can be determined event by event.

Our goal is to achieve a sensitivity 10 times as high as that of COMPTEL. To attain this, we first developed a prototype of the Compton camera operating in the 0.1–0.9 MeV range consisting of a 10 cm × 10 cm × 8 cm micro-TPC and a 10 cm × 10 cm × 2.5 cm NaI(Tl) camera [5]. We showed that the direction and the energy of the incident gamma-ray can be determined event by event. Based on the prototype, we developed a larger size

*Corresponding author.
E-mail address: hattori@cr.scphys.kyoto-u.ac.jp (K. Hattori).

0168-9002/$ - see front matter © 2007 Elsevier B.V. All rights reserved.
doi:10.1016/j.nima.2007.08.039

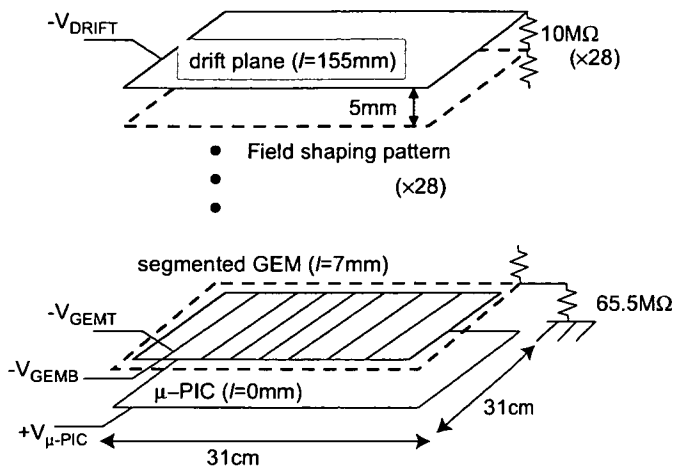

Fig. 1. Schematic representation of the micro-TPC. *l* indicates the vertical dimension.

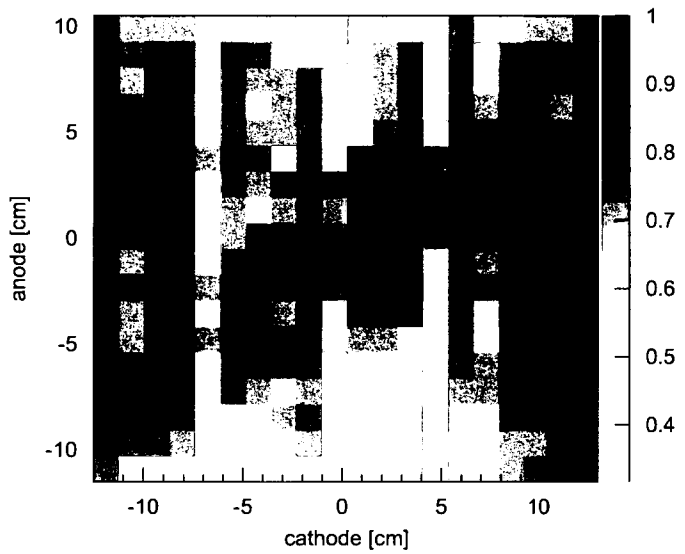

Fig. 2. Gainmap of the micro-TPC. The maximum gain was normalized to 1.

MeV-gamma-ray camera consisting of a 23 cm × 28 cm × 15 cm micro-TPC and a 37 cm × 37 cm × 2.5 cm NaI(Tl) camera. In this paper we present the results of the initial experimental evaluation of the large Compton camera.

2. Large size micro-TPC

We have developed a large size μ-PIC with a detection area of 31 cm × 31 cm [6] for use in the readout of the large size micro-TPC as shown in Fig. 1. The stable gas gain of the large μ-PIC was 2×10^3. However, a gas gain of 2×10^4

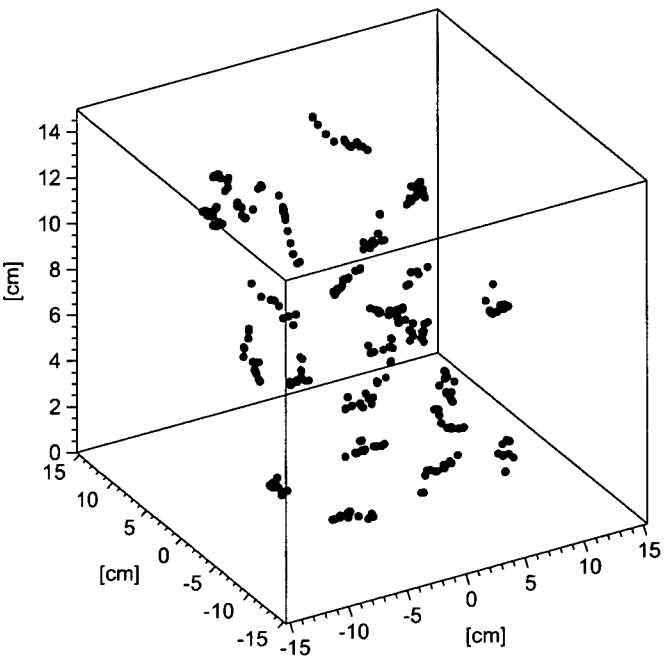

Fig. 4. Tracks of Compton recoil electrons in the micro-TPC irradiated with gamma-rays from the ^{137}Cs source.

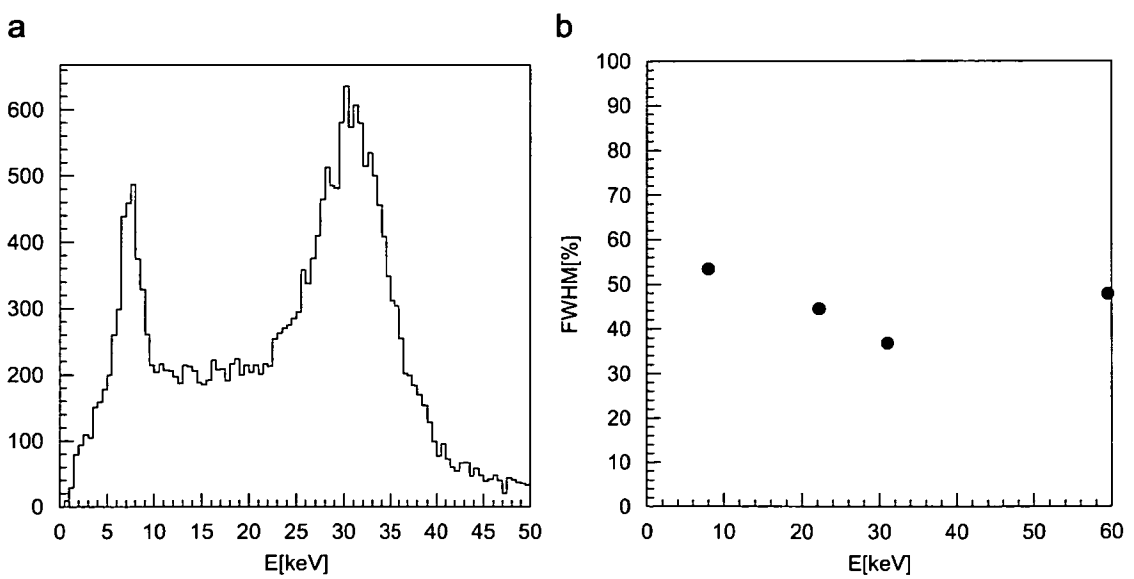

Fig. 3. (a) Spectrum of ^{133}Ba measured with the whole volume of the micro-TPC. (b) Energy resolutions of the micro-TPC.

is required to obtain clear tracks of recoil electrons. Therefore a combination of the μ-PIC and another electron multiplier was necessary. A Gas Electron Multiplier (GEM) [7], manufactured by Scienergy Co. Ltd. in Japan [8], was installed 7 mm above the μ-PIC. The GEM consists of a 50 μm thick kapton foil, and a copper cladding on each side where 70 μm holes are arranged in a hexagonal pattern with 140 μm between the centers. The detection area of the GEM was limited by the size of the material which the company was capable to handle. As a result, the sensitive area of the two-dimensional readout using the μ-PIC and the GEM was 23 cm × 28 cm. The GEM was segmented in eight regions in order to reduce its capacitance, because less capacitance reduces both current and damage caused by discharges. The electric field between the GEM and the μ-PIC was 1.4 kV/cm, and that in the drift region was 0.41 kV/cm. We achieved the stable gas gain of 2×10^4 using the combined system of the μ-PIC and the GEM, and this fulfilled the gas gain requirement.

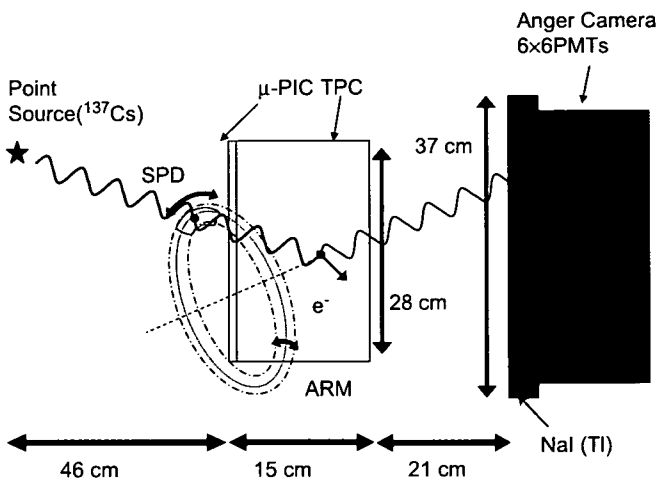

Fig. 5. Schematic representation of the Compton camera.

The micro-TPC was set in an aluminum vessel, the vessel was filled with $Ar-C_2H_6$ (90:10) gas to a pressure of 1 atm and then sealed for the duration of the measurements. The gas gain uniformity of the combined system was 13.9% RMS, as shown in Fig. 2. This was measured using 22.2 keV (^{109}Cd) X-rays at a total gas gain of 1×10^4 (μ-PIC 1.5×10^3, GEM 7). Fig. 3(a) shows a typical spectrum of X-rays obtained by the irradiation with ^{133}Ba. We can see the peak of the direct X-rays at 31 keV and that of the copper fluorescent X-rays at 8.0 keV, generated at the GEM and the μ-PIC by the original X-rays from ^{133}Ba. The energy resolution of the micro-TPC was measured to be 37% FWHM at 31 keV. This depended on the X-ray energy as shown in Fig. 3(b): below 31 keV the energy resolution improved with increasing energy. However, it was worse at 59.5 keV. This might be because of saturation effects in the preamplifiers. The situation is considered to worsen at higher energy, as more charges are presented to the preamplifiers.

In a previous measurement with 31 keV X-rays the energy resolution of the micro-TPC was worse, it was at about 60% FWHM, as described in Ref. [9]. Further modifications in the μ-PIC improved the gas gain uniformity, and therefore the better energy resolution of 37% FWHM was obtained.

The output charges of the 768 + 768 channels are pre-amplified, shaped and discriminated by ASD chips [10]. Using the discriminated signals, the three-dimensional tracks of charged particles are reconstructed. Clear tracks of cosmic muons were observed at a total gas gain of 3.0×10^4 (1.5×10^3 of the μ-PIC, 20 of the GEM). The spatial

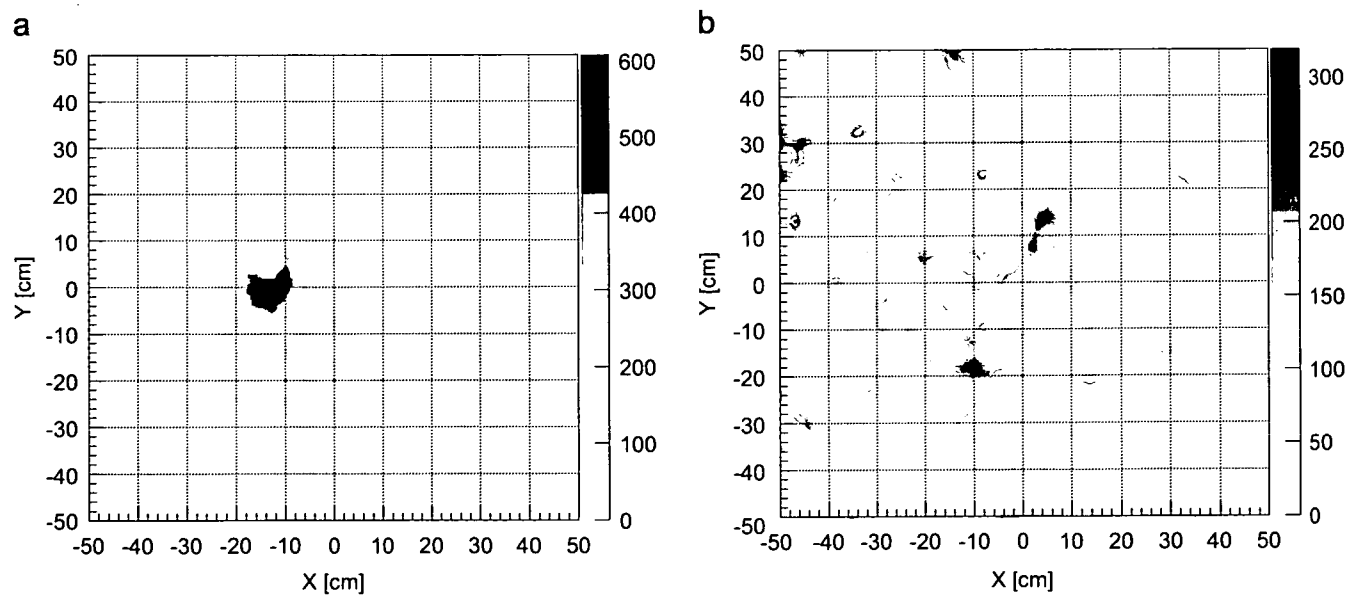

Fig. 6. Reconstructed images of incident gamma-rays from a ^{137}Cs (1 MBq) source. The center of the μ-PIC is (0 cm, 0 cm). (a) The source position is (−14 cm, 0 cm). (b) The positions of two sources are (−10 cm, −20 cm) and (5 cm, 15 cm), respectively.

resolution of the muon tracks was $\sqrt{0.56^2 + 0.31^2 z}$ (mm), where z was the drift length. Fig. 4 shows typical recoil electron tracks obtained by irradiating with ^{137}Cs. We find that the electrons were multi-scattered in the gas.

3. Large size Compton camera

Here, we describe the performance of the large size Compton camera. As shown in Fig. 5, it is built using the micro-TPC and the NaI(Tl) Anger camera. The size of the NaI(Tl) camera was 37 cm × 37 cm × 2.5 cm. The details of the scintillation detector are described elsewhere [11].

The micro-TPC was operated at a gas gain of 2×10^4 (2×10^3 of the μ-PIC, 10 of the GEM). The Compton camera was irradiated with 662 keV gamma-rays by a ^{137}Cs source from a distance of approximately 46 cm, and the reconstructed image is shown in Fig. 6(a). The ^{137}Cs source position was (−14 cm, 0 cm), the center of the μ-PIC was (0 cm, 0 cm). The reconstructed directions of the detected photons were concentrated on the position of the source. Fig. 6(b) shows the reconstructed images of two ^{137}Cs point sources, and we succeeded in separating them.

The angular resolution of advanced Compton imaging is defined by two angle parameters as shown in Fig. 7. One is the "angular resolution measure" (ARM) related to the angle between the scattered gamma-ray and the recoiled electron. This can be obtained in two ways, from kinematics and from geometry. ARM is the difference between these values. The other parameter is the "scatter plane deviation" (SPD), which is the determination accuracy of the plane formed by the scattered gamma-ray and the recoiled electron. Fig. 8 shows the distributions of ARM and SPD obtained for the data corresponding to Fig. 6(a), and the FWHM resolutions of ARM and SPD are 9.3° and 158°, respectively. In the case of the prototype with a 10 cm × 10 cm × 8 cm micro-TPC, the FWHM resolutions of ARM and SPD were typically 9° and 90°, respectively. Therefore, the ARMs of the large Compton camera and of the prototype were almost the same; however, the SPD of the large camera was greater. The SPD is determined by the accuracy of measuring the directions of the recoil electrons. If the signal-to-noise ratio of the large micro-TPC is improved, this accuracy also improves because more precise measurements for the tracks of the recoil electrons can be obtained. In the case of the prototype, the accuracy was better because the signal-to-noise ratio was better.

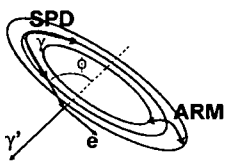

Fig. 7. The schematic view of ARM and SPD.

For the 662 keV gamma-rays, the measured detection efficiency was 2×10^{-6}. The low gamma-ray detection efficiency was caused mainly by the low detection efficiency of high-energy (> 100 keV) recoil electrons. However, the volume of the micro-TPC is large enough for even 300 keV electrons to transfer all the energy to the gas in the micro-TPC. It is thought that there are two reasons for the low detection efficiency of the high-energy recoil electrons. One is the small solid angle coverage of the scintillation detector, placed at 21 cm distance from the micro-TPC as shown in Fig. 5. This means that it detected mainly low-angle scattered gamma-rays, and the majority of the Compton-scattered gamma-rays escaped the detection. The low-angle scattered gamma-rays transfer only low energy to the recoil electrons. Correspondingly, high-energy recoil electrons in the micro-TPC do not coincide with hits in the scintillation detector. This will be improved by enlarging the solid angle coverage of the scintillation detector.

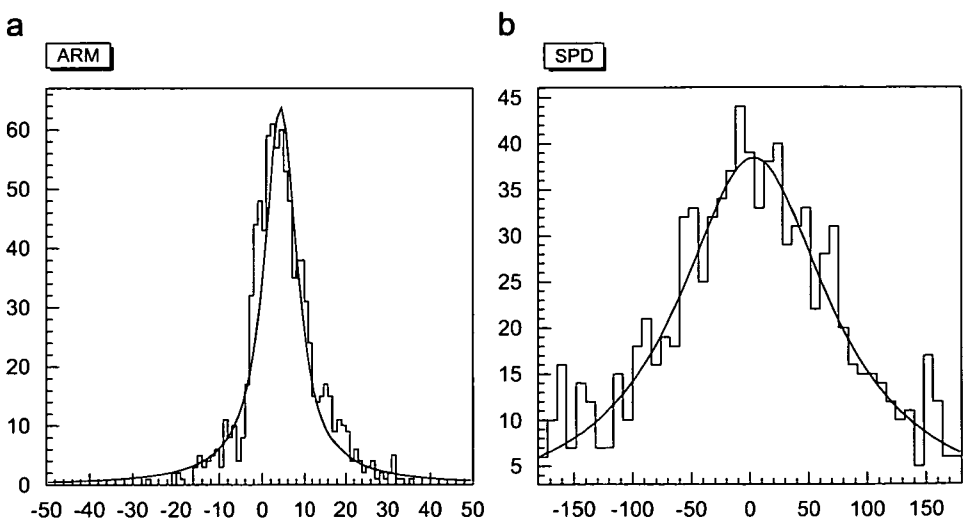

Fig. 8. (a) and (b) show the distributions of ARM and SPD for 662 keV gamma-rays, respectively. The solid lines are the best-fit Lorentzian.

The second reason is ascribed to the saturation effects in the preamplifiers, as described in the previous section. They cause a deteriorated energy resolution of the recoil electrons at higher energies, what also leads to a low gamma-ray detection efficiency due to a background rejection algorithm. This is based on a consistency check where the alpha-angle (the angle between the recoil electron and the scattered gamma-ray), as derived by kinematics from the energies of the recoil electron and of the scattered gamma-ray, is compared to the angle which is geometrically deduced from the directions of the recoil electron and of the scattered gamma-ray [2]. Compton events with a large difference of the two angles were rejected. Consequently, we have developed new ASD chips with a wider dynamic range to avoid the saturation in the preamplifiers.

4. Conclusion

We have developed a micro-TPC, based on the μ-PIC with a detection area of 30 cm × 30 cm and a GEM with a detection area of 23 cm × 28 cm, the drift length was 15 cm. The combination of the μ-PIC and a GEM realized stable operation of the chamber at a gas gain of 2×10^4, and this was adequate to obtain tracks of minimum ionizing particles and thus of recoil electrons. Then, the performance of the Compton camera (consisting of the micro-TPC and the Anger camera) was investigated by irradiating with 662 keV gamma-rays from a ^{137}Cs source. We succeeded in reconstructing recoil electrons recorded with the micro-TPC and we obtained fine images of different point sources.

References

[1] V. Schoenfelder, et al., Astrophys. J. Suppl. Ser. 86 (1993) 657.
[2] R. Orito, et al., Nucl. Instr. and Meth. A 513 (2003) 408.
[3] T. Tanimori, et al., New Astron. Rev. 517 (2004) 241.
[4] A. Ochi, et al., Nucl. Instr. and Meth. A 471 (2001) 264.
[5] T. Tanimori, et al., New Astron. Rev. 48 (2004) 263.
[6] A. Takada, et al., Nucl. Instr. and Meth. A 573 (2007) 195.
[7] F. Sauli, Nucl. Instr. and Meth. A 386 (1997) 531.
[8] M. Inuzuka, et al., Nucl. Instr. and Meth. A 525 (2004) 529.
[9] K. Miuchi, et al., Nucl. Instr. and Meth. A 576 (2007) 43.
[10] H. Kubo, et al., Nucl. Instr. and Meth. A 513 (2003) 94.
[11] R. Orito, et al., 2005 IEEE Conference Record, vol. 1, 2005, pp. 443–447.

資料 18

資料(19)

Available online at www.sciencedirect.com
ScienceDirect
Nuclear Instruments and Methods in Physics Research A 581 (2007) 110–114
NUCLEAR INSTRUMENTS & METHODS IN PHYSICS RESEARCH Section A
www.elsevier.com/locate/nima

Response of a Micro Pixel Chamber to heavy ions with the energy of several hundreds of MeV/n

Tsutomu Nagayoshi[a,*], Tadayoshi Doke[a,d], Yasunobu Fujita[a], Kaori Hattori[b], Koji Ishida[a], Jun Kikuchi[a], Hisashi Kitamura[e], Tatsuto Komiyama[d], Hidetoshi Kubo[b], Haruhisa Matsumoto[d], Kentaro Miuchi[b], Hironobu Nishimura[b], Kiwamu Saito[c], Shin-ichi Sasaki[c], Hiroyuki Sekiya[b], Atsushi Takada[b], Toru Tanimori[b], Kazuhiro Terasawa[a,d], Hiroko Tawara[c], Yukio Uchihori[e], Kazuki Ueno[b]

[a]*Waseda University, 17 Kikuicho, Shinjuku-ku, Tokyo 162-0044, Japan*
[b]*Kyoto University, Kitashirakawa-oiwakecho, Sakyo-ku, Kyoto 606-8502, Japan*
[c]*High-Energy Accelerator Research Organization (KEK), 1-1 Oho, Tsukuba, Ibaraki 305-0801, Japan*
[d]*Japan Aerospace Exploration Agency (JAXA) 2-1-1 Sengen, Tsukuba Ibaraki 305-8505, Japan*
[e]*National Institute of Radiological Sciences (NIRS), 4-9-1 Anagawa, Inage-ku, Chiba 263-8555, Japan*

Available online 26 July 2007

Abstract

Beam tests were performed for a Micro Pixel Chamber (μ-PIC) with a detection volume of $10 \times 10 \times 10\,cm^3$ to investigate the response to heavy ions. The three-dimensional tracks of carbon, silicon, and iron beams were successfully observed and their track lengths were measured. Additionally, Linear Energy Transfer (LET) distributions of each ion were obtained, and the mean LET values were consistent with the theoretical calculation of mass stopping power within an error of ~10%. This detector is a candidate for an ideal dosimeter in space.

PACS: 29.40.Cs; 29.40.Gx

Keywords: Gaseous detector; Micro-Pattern detector; Position sensitive; TEPC; LET; Heavy ions

1. Introduction

We have been developing the position sensitive gaseous detector named "Micro Pixel Chamber (μ-PIC)" [1], which is categorized as a micro-pattern gas detector. The μ-PIC consists of a double-sided printed circuit board (PCB) with pixel-like electrodes. The anode and cathode strip electrodes are orthogonally arranged with a pitch of 400 μm on both sides of the 100 μm thick polyimide insulation layer. Each cathode strip has 260 μm diameter openings with a pitch of 400 μm. Pixel-like anode electrodes of 60 μm are also formed at the center of each cathode hole penetrating the insulator. Our μ-PIC has 256 anode and 256 cathode strips, and the detection area is $10 \times 10\,cm^2$. The μ-PIC has the following features:

(1) no charging-up of positive ions on the insulator surface,
(2) little fluctuation of gas gain in whole detection area (<4% RMS for $10 \times 10\,cm^2$ detection area),
(3) two-dimensional fine position resolution (120 μm RMS),
(4) high gas gain (~7000) without any other additional gas multiplication devices,
(5) mass production capability.

The main use of the μ-PIC is the 3D imaging of charged particles. For this purpose, μ-PIC is operated as a readout of a Time Projection Chamber (TPC) named the "μ-TPC" [2], which has an $11 \times 11 \times 10\,cm^3$ drift space. Fig. 1 shows

*Corresponding author. Tel./fax: +81 3 3203 4379.
E-mail address: nagayosi@kurenai.waseda.jp (T. Nagayoshi).

0168-9002/$ - see front matter © 2007 Elsevier B.V. All rights reserved.
doi:10.1016/j.nima.2007.07.040

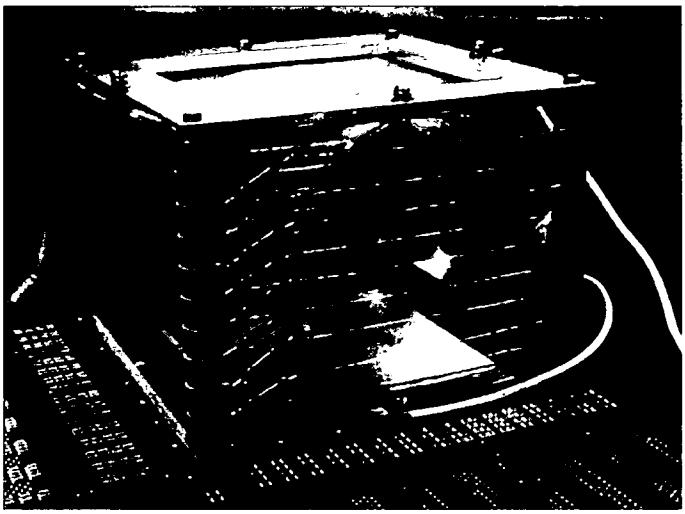

Fig. 1. Photograph of a μ-PIC with an 11 × 11 × 10 cm³ drift cage.

a photograph of the μ-TPC. The 0.5 mm diameter field wires are arranged with a pitch of 1 cm. Resistances of 10 MΩ are connected between two adjacent field wires. Ionization electrons drift to the plane of μ-PIC and the two-dimensional position is detected by anode and cathode electrodes. The z-position is then measured from the information of known drift velocity of electrons and the drift time. According to former experiments with proton tracks of ~1 GeV, the 3D position resolution of less than 300 μm was achieved.

Originally, we have been developing the μ-TPC for the application of gamma-ray imaging onboard a satellite, based on tracking of Compton scattered electrons [3]. Because the typical energy of a scattered electron is 1 MeV—the MIP energy region—, high gas gain operation ($>10^4$) is needed. Heavy ions in cosmic-rays might be a serious problem for the detector. Ionization in the detector due to cosmic-ray particles creates an enormous number of electron–ion pairs, which might cause discharges [4]. Therefore, the influence of the heavy ion irradiation to the μ-TPC should be studied to ensure stable operation of the detector in a space environment.

When astronauts work in a space environment like the International Space Station (ISS) or manned exploration to the Moon or Mars, exposure to cosmic radiation including extremely large solar flares sometimes gives the large risk to the crew. The μ-TPC is a candidate of an ideal dosimeter in space as a LET spectrometer. The details for space dosimetry are described elsewhere [5]. In this case, a gas gain of 100 to 1000 is needed to measure the LET of heavy ions.

For these purposes, it is necessary to evaluate the response of the μ-TPC to heavy ions. We performed irradiation tests for a μ-TPC using the heavy ion accelerator at National Institute of Radiological Sciences (NIRS) in Japan. In this paper, we describe the heavy ion irradiation test and discuss the response of the μ-TPC.

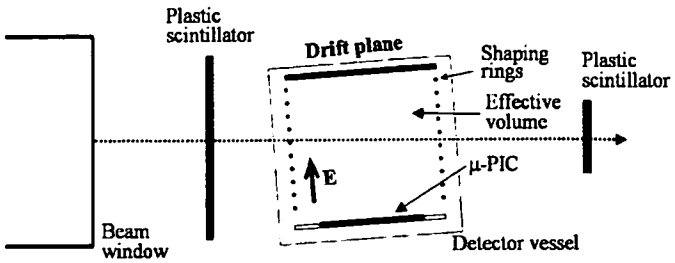

Fig. 2. Set-up of the μ-TPC at the HIMAC beamline. The trigger scintillators are also shown. The beam penetrates this set-up horizontally.

2. Heavy ion irradiation experiment at HIMAC

The beam experiments were carried out at the Heavy-Ion Medical Accelerator in Chiba (HIMAC) of NIRS. The beam energies were 400 MeV/n for carbon ions, 800 MeV/n for silicon, and 500 MeV/n for iron ions, because the typical energy of heavy ions in cosmic ray is 100 MeV to 1 GeV [6].

The experiment setup at the beamline is shown in Fig. 2. The detector was inclined at 5° against the horizontal in order to evaluate the Z direction of the beam tracks. One scintillation counter was placed in front of and one behind the μ-TPC. The data acquisition system was triggered by coincidental hits from both scintillators. These triggering signals are produced when a particle passes through the whole detector system.

The drift volume was filled with a gas mixture of the Ar/C_2H_6(90/10) at 1 bar, and a drift voltage of 2000 V was applied on the top of the drift cage. The corresponding drift electric field was 0.2 kV/cm. The drift velocity of electrons in the gas mixture was 4.5 cm/μs at the drift electric field [7].

An ^{241}Am α source was deposited on the top plane of the drift cage for an energy calibration. To restrict the intensity of the irradiation the α source was placed 5 mm above the drift plane and collimated by a 2 mm diameter hole at the center of the drift plane. The total energy deposit of α particles in the detection volume of the μ-TPC was effectively 5 MeV.

The ionization electrons drift to the μ-PIC plane along the lines of electric force and are multiplied in the neighborhood of the anode pixels. The strip electrodes are connected to the Amplifier Shaper Discriminator (ASD) chips of a time constant of 80 ns [8]. The digital signals from the ASD chips are fed to the front-end position encoding module (PEM) based on five Field Programmable Gate Arrays (FPGAs). The hit positions of the electrodes are encoded as a three-dimensional image. Thus the three-dimensional track is reconstructed using the clock information together with the X- and Y-information. To analyze the pulse shape from the anode, all analog signals from the ASDs are summed up into one channel which is fed to a 100 MHz flash ADC (FADC). The energy deposit of each incident particle is

calculated from the integrated wave form using the calibration data.

3. Results and discussion

The μ-PIC was stable during operation at a gas gain of ~100 even for an iron beam which had the highest energy deposit. There was no gas gain variation between before and after the irradiation.

The beam profiles for carbon, silicon, and iron ions have similar shapes with a 10 mm diameter. Fig. 3 shows the detected three-dimensional tracks for a silicon beam. This is composed of the superposed images of 50 tracks. The cross-sectional views for three beam profiles are given in Fig. 4 with their projections to the horizontal and the vertical axes. In this figure, the absolute value in the x-axis is insignificant and only the width of the distribution can be evaluated. The shapes of the beam profiles are properly reconstructed, compared with the beam profile monitor just before the end window of the beam line. The width of the histogram for each projection was consistent with the size of beam profile.

The reconstructed tracks were shown as a sequence of points produced by a timing of the clock frequency in the data acquisition system. Each sequence of points was fitted by a three-dimensional linear function. The track length is defined as the length along this function from an end to another end in the effective drift region. The distribution of the track lengths are shown in Fig. 5. The difference in the

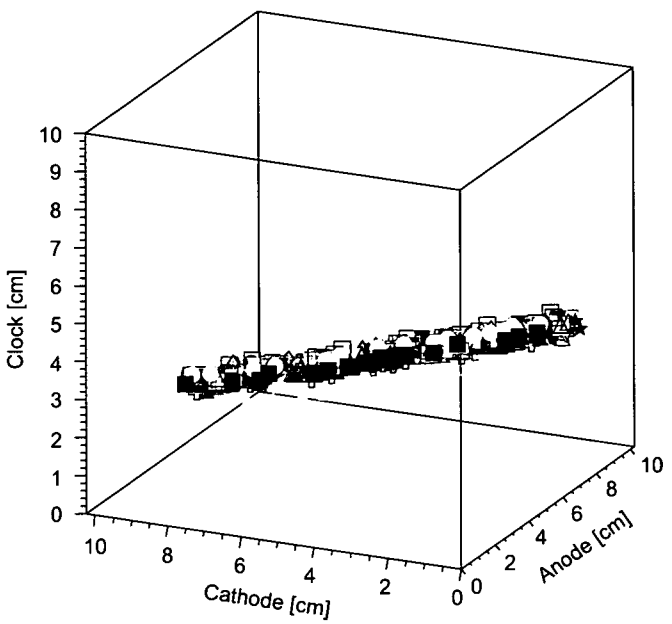

Fig. 3. Reconstructed three-dimensional image of Si tracks in the Ar/ethane (90/10) gas. One hundred tracks are superimposed in the figure.

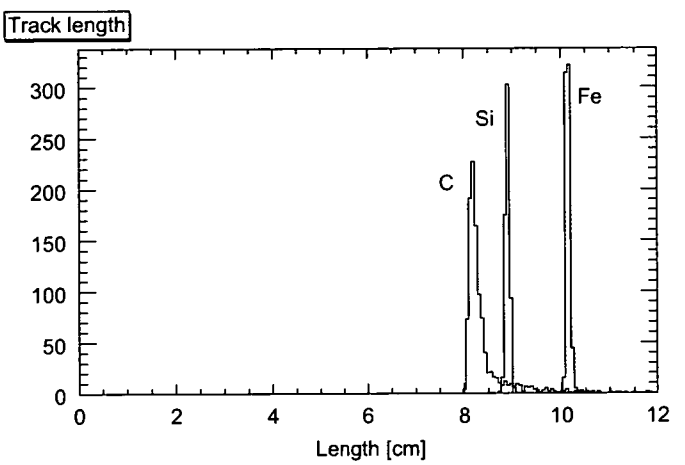

Fig. 5. Distribution of each track length for carbon, silicon, and iron beams.

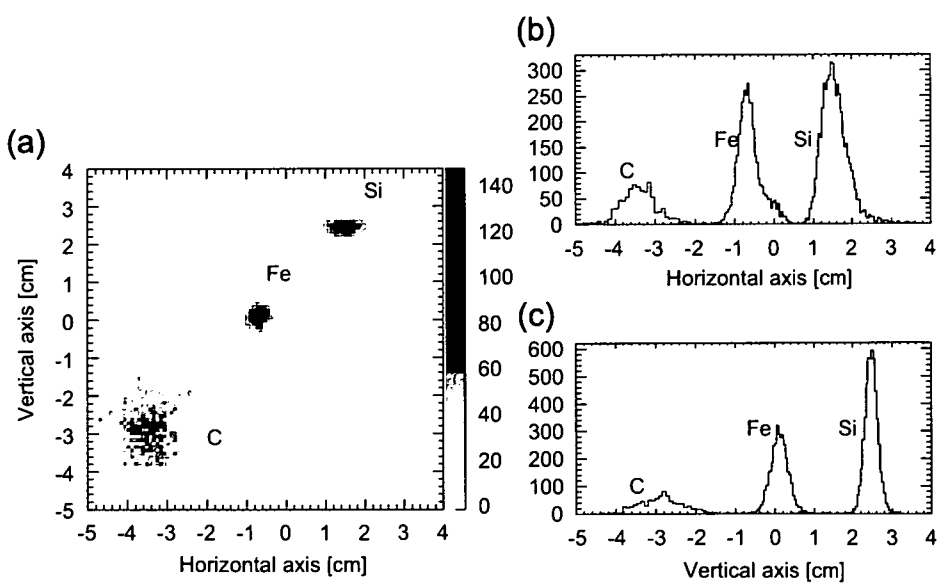

Fig. 4. Reconstructed beam profiles for carbon, silicon, and iron ions (a) and their projections to horizontal (b) and vertical axes (c).

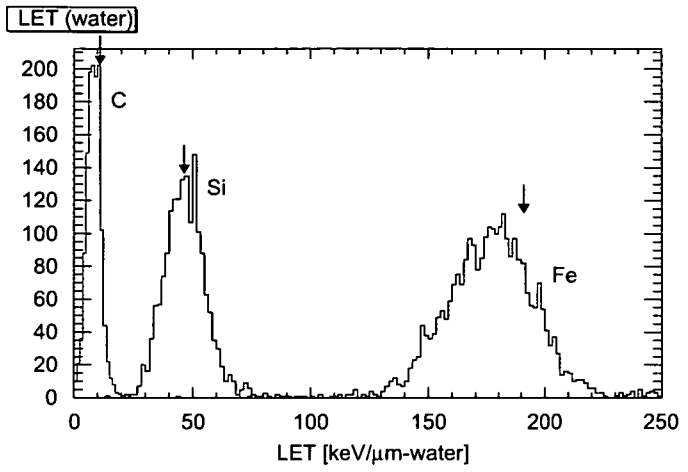

Fig. 6. LET distribution of carbon, silicon, and iron ion tracks. The arrows shows the results of theoretical calculation.

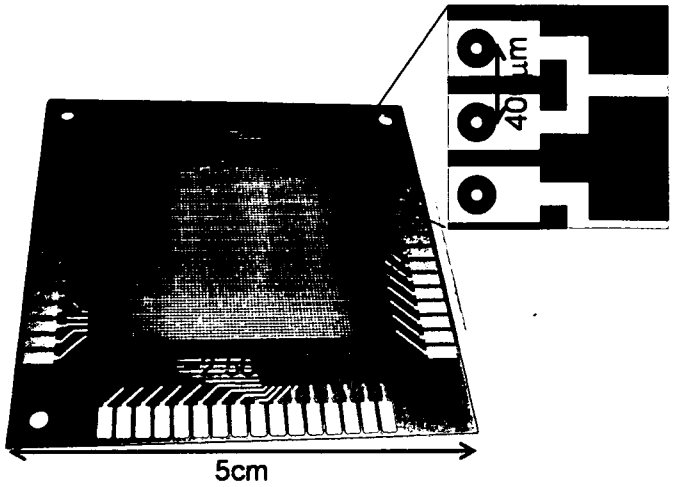

Fig. 7. Photograph of a μ-PIC with the size of 2.6 × 2.6 cm^2 together with the schematic drawing of the electrodes.

track length is consistent with the setup of each experiment. In this case, a dead layer existed in the effective volume. Therefore, the track length was less than 11 cm. The small tail for carbon ions is due to some noise events affecting the fitting process. Taking these reasons into consideration, these results are satisfactory.

We need to measure the LET of each particle for space dosimetry; in particular, the LET in water is essential. The distribution of energy deposits of each ion is also obtained as well as the track length [9]. LET for each event was calculated by energy deposit and track length. Fig. 6 shows the LET distributions for three kinds of ions. The theoretical values calculated by SRIM program [10] are also shown as arrows in this figure. The following equations were used to obtain the LET for water from that for Ar/ethane gas.

$$\mathrm{LET}_{\mathrm{water}}\ [\mathrm{keV}/\mu\mathrm{m}] = \mathrm{LET}_{\mathrm{Ar/ethane}} \times 1.28 \times 1.00/(1.62 \times 10^{-3}) \quad (1)$$

$$\mathrm{LET}_{\mathrm{Ar/ethane}} = (\text{energy deposit})/(\text{track length})\ [\mathrm{keV}/\mu\mathrm{m}]. \quad (2)$$

Here, $\mathrm{LET}_{\mathrm{water}}$ is the LET for water and $\mathrm{LET}_{\mathrm{Ar/ethane}}$ is that for the Ar/ethane (90/10) gas mixture. The conversion factor corresponding to the ratio of the mass stopping power of water for relativistic particles to that of Ar/ethane is 1.28. The density of water is 1.00 and that of 1 bar Ar/ethane is 1.62×10^{-3}. The difference between theoretical and experimental LET values of carbon was about 10%. The mean LET value for each distribution of silicon and iron was consistent with the theoretical values of the mass stopping power within an error of about 5%.

4. Summary and future prospect

Irradiation tests of a μ-TPC with an effective volume of 10 × 10 × 10 cm^3 were performed using heavy ion beams at HIMAC of NIRS in Japan. The μ-PIC was stably operated for the heavy ion irradiation. Three-dimensional tracks of carbon, silicon, and iron ions were successfully measured. Their track lengths and energy deposits in the detector were also measured. Finally, we evaluated the LET value for each particle and found the values to be consistent with the theoretical calculation within an error of 10%. This is essential for the LET spectrometer in space. In this paper, we established the principle of the cosmic-ray dosimeter based on the μ-PIC.

For utilization in space, the robustness of the μ-PIC for heavy ion irradiation has to be checked. The response of the μ-PIC to heavy particles is important for high gas gain ($> 10^4$) operations like cosmic MeV gamma-ray observation. A dosimeter for space applications must be small so it can be installed on a spacecraft. A smaller size μ-PIC has recently been manufactured in order to develop a new space dosimeter. Fig. 7 presents a photograph of a μ-PIC with an effective area of 2.6 × 2.6 cm^2. In the new design, the 400 μm pitch electrodes are connected with the adjacent strips as shown in Fig. 7, and the net electrode pitch is 800 μm. The position resolution obtained from the pitch is adequate for space dosimetry based on the results of Real-time Radiation Monitoring Device-III (RRMD-III) [11]. Furthermore, the detector should be made from tissue equivalent materials. In the near future, we will make the dosimeter with a tissue equivalent wall and a tissue equivalent gas.

Acknowledgments

This study is being carried out as a part of "Ground Research Announcement for Space Utilization", promoted by the Japan Space Forum. T. Nagayoshi is supported by Research Fellowships of Japan Society for the Promotion of Science for Young Scientists.

References

[1] A. Ochi, et al., Nucl. Instr. and Meth. A 471 (2001) 264;
T. Nagayoshi, et al., Nucl. Instr. and Meth. A 513 (2003) 277;
T. Nagayoshi, et al., Nucl. Instr. and Meth. A 525 (2004) 20.